Joint Reconstruction and Registration Using Level Sets: Application to the Computer-guided Ablation of Atrial Fibrillation

Jonghye Woo[1], Byung-Woo Hong[2], Sunil Kumar[3], Indranill Basu Ray[4] and C.-C. Jay Kuo[1]

[1]Department of Electrical Engineering, University of Southern California, Los Angeles, CA 90089-2564
[2]Computer Science Department, University of Los Angeles, Los Angeles, CA 90095
[3]Electrical and Computer Engineering Department, San Diego State University, San Diego, CA 92182
[4]School of Medicine and Dental Sciences, State University of New York at Buffalo, Buffalo, NY 14214
jonghyew@usc.edu, hong@cs.ucla.edu, skumar@mail.sdsu.edu
indranillbasuray@yahoo.com, cckuo@sipi.usc.edu

Abstract

Use of 3D reconstructed cardiac images generated from Magnetic Resonance Imaging (MRI) and Computed Tomography (CT) play an important role in percutaneous image guided interventions. Image integration technique using these 3D images is especially useful for guiding a number of interventional therapies used to treat cardiac arrhythmias. This paper presents an implicit surface reconstruction and registration method based on a variational and partial difference equation (PDE) method for the use of catheter ablation. Our optimal shape representation is based on the Electroanatomic mapping (EAM) data and a shape prior, and level set framework is incorporated for taking cardiac deformation and noise into account. We propose a novel image integration method which enables reconstruction and registration under non-rigid deformation simultaneously. Promising experimental results show the potential of our approach.

1. Introduction

Atrial fibrillation (AF) is the most common sustained cardiac arrhythmia encountered in clinical practice. In the United States alone, there are over 3.5 million patients with this disorder [16]. Atrial fibrillation can result in serious complications, including congestive heart failure and thromboembolism. Despite the advances, drug therapy for controlling this disease is still unsatisfactory. This has led to the use of novel non-pharmacological, interventional approaches based on creating percutaneous catheter based lesion inside the heart. Lesions are delivered in the left atrial-pulmonary vein junction with an aim to electrically isolate these veins from the rest of the atrium. This, in effect, protects the atrium from the fast heartbeats originating in the veins that both initiate and perpetuate atrial fibrillation.

The present day procedure for interventional treatment of atrial fibrillation entails mapping the left atrium and the attached pulmonary veins using an Electroanatomic mapping (EAM) system and this mapping information is used to deliver lesions as well. One important limitation of this system is its inability to create the anatomy. Instead a virtual shell is created to represent the atrial wall and the vein. The points on the atrial wall where the catheter is manually touched is used to create this shell [14]. This process can be made more precise if a real anatomy is used instead of the virtual shell. Thus to make use of the real anatomy, the images from MRI/CT and the data from EAM systems are integrated into the canonical reference frame.

Image integration process for the heart aims to provide an anatomical, physiological and functional representation combining anatomical surface model that is formed by MRI/CT images and localized electrical information that is measured by EAM systems. This representation is of great use for an organ like the heart; which is an electromechanical organ, where electrical stimulus drives mechanical contractions. Clinical procedures such as catheter ablation can be made more precise with the help of image integration as both the anatomical and electrical information is then available to the operator which ensures both safe catheter maneuverability and enables delivery of effective lesions with minimal collateral damage and complications. This is particularly important while doing ablations in a complex structure like the left atrium that is surrounded by important organs that are vulnerable to damage if lesions are not appropriately directed with close anatomical guidance. Furthermore, even the pulmonary veins themselves are liable

to be damaged with grave long-term consequences if the lesions extend deep into them instead of being restricted to the ostia. Given the limited area where lesions need to be delivered, it becomes important that a precise anatomy is available to the operator to achieve this. Thus very precise image integration is of utmost importance in such cases.

In registration process, one obvious difficulty stems from the noises or outliers that are inevitably associated with the MRI/CT imaging process and the EAM data collection procedure. Unlike other organs in the body, heart undergoes contractile motion, apart from the respiratory motion, thus making it unique and very challenging to register and integrate with other modalities. These motions, in addition to physiological variations including changes in heart rate, heart rhythm and respiratory effect, are the sources of outliers.

In this paper, we propose a variational framework for a 3D surface reconstruction algorithm based on the level set method which provides an implicit and topology free shape representation. Our goal is to reconstruct the anatomical heart surface from sparse and noisy EAM data points by incorporating a heart shape model from MRI/CT reconstruction as a prior information. By leveraging a heart shape model, we can compensate for the incomplete EAM data thereby representing the true anatomical heart more specifically.

The proposed method has following strengths: (1) it is robust with respect to non-rigid deformation caused by cardiac motion and noise, and (2) it can construct the optimal surface without explicit correspondences between the MRI/CT surface and EAM data points due to our implicit surface representation.

2. Related Work

Developing a computer-guided system for ablative heart surgery involves the image registration or integration techniques which are usually performed assuming rigid transformation between pre-operative MRI/CT reconstruction and intra-operative EAM data points [17, 7]. Among various registration algorithms, Iterative Closest Point (ICP) method and its variants have been widely used for this application due to their computational efficiency [11].

The ICP algorithm starts with two meshes and an initial guess for their relative rigid-body transform, and iteratively refines the transform by repeatedly generating pairs of corresponding points on the meshes and minimizing an error metric [2]. The standard ICP algorithm, however, does not take the outliers into account. To mitigate this problem, various modified ICP methods have been proposed [19]. Especially the method that rejects pairs is closely related to dealing with outliers. The purpose of this is to remove outliers which may affect the performace substantially. The popular approach to find outliers is to use threshold such as certain constant, fraction of sorted distance and some multiple of standard deviation of distance [4, 15, 12]. Still, with these variants, it is challenging to deal with non-rigid deformation and distinguish inliers from outliers.

Most of previous schemes used ICP-based method and did not address the problem mentioned above; the rigid transformation has difficulty in dealing with outliers and non-rigid deformation. Instead, they focused on the clinical registration strategy. For example, Reddy, et al. have shown the feasibility of combining MRI with CARTO-XP in a porcine model of myocardial infarction (MI) [17, 11]. They used mICP (Modified Iterative Closest Point) scheme for registration which does not address the outlier problem. Clinical registration strategy combining landmark and surface registration has been proposed in [7]. This study assessed the accuracy for each cardiac chamber by using different clinical registration method, which does not mention the problem above as well. Recent research shows that the size of left atrium affects the accuracy [9]. The patient who has big chamber volume tends to have more ablation errors.

However, the assumption made by the above schemes regarding the undergoing transformation is deficient and usually results in unsatisfactory results since a non-rigid deformation is involved between the anatomical heart model reconstructed from MRI/CT images and temporal instances of the heart at the collection of EAM data points. This physiological and anatomical variation that occurs in the formation of the heart surface model and the collection of EAM data points naturally requires to allow a non-rigid transformation or equivalently diffeomorphism between the model and the data.

In order to overcome such limitations with clinical registration approaches based on a rigid-transformation, we consider this registration problem as a 3D surface reconstruction method from EAM data points incorporating a given surface model. Our approach is related to the problem of surface reconstruction from point clouds which arises in situations such as scanning noisy image and 2D slices of medical images. A surface reconstruction using explicit representation has been proposed in [18]. However, it is requried to parameterize the arbitrary point set, which makes it difficult to deal with. In [8, 1] other approaches based on Delaunay triangulations and Voronoi diagrams have been proposed to construct triangulated surfaces. These approaches require to find the right connection among the point sets, which is difficult when it comes to noisy and unorganized point set. Recently, the methods based on implicit shape representation using level set have been proposed [5, 6, 13]. The non-parametric, implicit approach has advantages in that it can deal with arbitrary toplogy change and represent deformation. Hoppe et al. proposed an algorithm for reconstructing the surface using signed distance function from

unorganized points in [10]. Hongkai Zhao, et al. proposed the novel approach using unsigned distance function and weighted minimal surface to reconstruct the surface in [23]. However, these algorithms are only restricted to cases when the population of points is regularly dense enough to characterize the desired surface and thereby they are not applicable to our application where EAM data points are sparse and insufficient. Thus our reconstruction algorithm for a 3D heart surface (Left Atrium and its pulmonary veins) from insufficient EAM data points incorporates a given heart shape model formed by MRI/CT images. The optimal surface is obtained by minimizing the energy functional that consists of a data fitting term and a prior knowledge term.

3. Simultaneous Reconstruction and Registration Model

In this section we present our framework for simultaneous reconstruction and registration algorithm based on the level set method. Our surface reconstruction problem from EAM data points incorporating a heart surface model obtained by MRI/CT images is first formulated in a variational setting followed by its numerical implementation.

3.1. Variational Methods and Bayesian Inference

Let us denote the evolving surface $S(x),\ x \in \Omega$ as the zero level set of an embedding function $\phi(x) = \Omega \rightarrow \mathbb{R}$ as given by [20]:

$$\begin{cases} S = \{x \in \Omega \mid \phi(x) = 0\}, \\ interior(S) = \{x \in \Omega \mid \phi(x) > 0\}, \\ exterior(S) = \{x \in \Omega \mid \phi(x) < 0\}. \end{cases} \tag{1}$$

The desired surface S to reconstruct is replaced by the unknown function ϕ in the formulation and a signed distance function is employed for ϕ. We also introduce the heaviside function H and Dirac measure δ as defined by:

$$H(x) = \begin{cases} 1, & x \geq 0 \\ 0, & x < 0 \end{cases}, \qquad \delta(x) = \frac{d}{dx} H(x). \tag{2}$$

The shape of the desired surface $S(x)$ is represented by $S(x) = H(\phi(x))$. Similarly, a given shape model $M(x),\ x \in \Omega$ obtained from MRI/CT images is represented by the heaviside function $M(x) = H(\psi(x))$ where $\psi(x)$ is a level set function as given by:

$$\begin{cases} M = \{x \in \Omega \mid \psi(x) = 0\}, \\ interior(M) = \{x \in \Omega \mid \psi(x) > 0\}, \\ exterior(M) = \{x \in \Omega \mid \psi(x) < 0\}. \end{cases} \tag{3}$$

Let us denote a set of given unorganized EAM data points as:

$$D = \{p_1, p_2, \ldots, p_n\} \subset \mathbb{R}^3 \tag{4}$$

where n is the number of given points. Then, we reconstruct a 3D surface S by finding function ϕ that minimizes functionals of the form

$$E(\phi) = E_{point}(\phi, D) + \alpha E_{prior}(\phi). \tag{5}$$

This cost functional consists of two components: The first term measures how well the surface is fitted to the points based on the distance between the surface and the points. The second term measures how plausible the surface is in terms of the prior knowledge on the desired surface. The parameter $\alpha \geq 0$ is a weighting constant that adjusts the importance of two factors. This variational approach is equivalent to the approach of Bayesian inference in a probabilistic framework and the desired surface S is obtained by maximizing the following posterior probability:

$$P(S|D) = \frac{P(D|S)P(S)}{P(D)} \tag{6}$$

where $P(D|S)$ is the likelihood function, $P(S)$ is the prior probability of the surface and the probability $P(D)$ can be simply considered as a constant. Maximizing this conditional probability with respect to the surface S for the data points D is equivalent to minimizing its negative logarithm:

$$-\log(P(S|D)) = -\log(P(D|S)) - \log(P(S)) + \mathrm{c} \tag{7}$$

where c is a constant. Then, we have $E_{point}(\phi, D) = -\log(P(D|S))$ and $\alpha E_{prior}(\phi) = -\log(P(S))$. The prior probability of the surface S can be expressed in terms of intrinsic and extrinsic prior knowledge on the surface. The intrinsic prior knowledge prefers a smooth surface for S penalizing large variations and the extrinsic prior knowledge attracts the surface S towards the given shape model M.

3.2. Energy Formulation

We assume that the desired surface S to reconstruct is likely to be close to the given surface model M and is also attracted toward the given data points D. The surface S is obtained by minimizing the energy functional that consists of a data fitting term and a prior knowledge term.

First, the data fitting term can be expressed as follows:

$$E_{point}(\phi|D) = \sum_{i=1}^{n} \int_{\Omega} |\phi(x) \cdot \delta(x - p_i)|^2 \, dx \tag{8}$$

where ϕ is a surface to be reconstructed and recall that ϕ is represented by a signed distance function. This term measures the Euclidean distance of each point p_i from the surface ϕ.

Secondly, we impose a prior knowledge on the surface S assuming that the surface prefers to be close to the given surface model M preserving geometrically smooth property that penalizes abrupt change of surface gradient. The energy for the prior knowleges consists of two terms: a smoothness regularization term and a shape dissimilarity term as follows:

$$E_{prior}(\phi) = E_{reg}(\phi) + E_{shape}(\phi|\psi) \tag{9}$$

where $H(\phi) = S$ and $H(\psi) = M$.

The smoothness regularization term can be expressed as

$$E_{reg}(\phi) = \int_{\Omega} |\nabla H(\phi(x))| dx \tag{10}$$

where H is the heaviside function. This term gives smoothness regularization by measuring the length of the shape in 2D and the area of the shape in 3D, respectively.

The shape dissimilarity term can be expressed as

$$E_{shape}(\phi|\psi) = \int_{\Omega} |H(\phi(x)) - H(\psi(T(x)))|^2 dx \tag{11}$$

where $T(x)$ is the rigid transformation including scaling, rotation and translation. This term measures the symmetric difference between $H(\phi)$ and $H(\psi)$ under the rigid transformation.

As mentioned earlier, the surface reconstruction energy functional can be formulated using the energy minimization problem as follows:

$$\phi^* = \arg\min_{\phi} E(\phi) \tag{12}$$

with a constraint $|\nabla\phi| = 1$ that is a property of the signed distance function, and the whole energy functional $E(\phi)$ can be defined as follows:

$$E(\phi) = E_{point}(\phi|D) + \alpha \left(E_{reg}(\phi) + E_{shape}(\phi|\psi)\right) \tag{13}$$

By adjusting α, we can control the degree of a data fitting term and a prior knowledge term. We can obviously apply different weights on E_{reg} and E_{shape}.

3.3. Numerical Implementation

For the numerical scheme, we used the following approximations for the heaviside and Dirac delta function as given in [3, 22]:

$$\delta(z) = \begin{cases} 0, \text{ if } |z| > \varepsilon \\ \frac{1}{2\varepsilon}\left[1 + \cos(\frac{\pi z}{\varepsilon})\right], \text{ if } |z| \leq \varepsilon \end{cases} \tag{14}$$

$$H(z) = \begin{cases} 1, \text{ if } z > \varepsilon \\ 0, \text{ if } z < -\varepsilon \\ \frac{1}{2}\left[1 + \frac{z}{\varepsilon} + \frac{1}{\pi}\sin(\frac{\pi z}{\varepsilon})\right], \text{ if } |z| \leq \varepsilon \end{cases} \tag{15}$$

Our energy functional can be minimized with respect to $\phi(x)$ using Euler-Lagrange equation. Following that the gradient descent method can be used to solve this equation numerically.

$$\begin{aligned} \frac{\partial\phi}{\partial t} = -2\sum_{i=1}^{n} \phi(x)\delta(x - p_i) + \alpha[\delta(\phi) div(\frac{\nabla\phi}{|\nabla\phi|}) \\ -2\int_{\Omega} (H(\phi) - H(\psi))\delta(\phi) dx] \end{aligned} \tag{16}$$

Solving this numerical method is often challenging due to the fact that the time step should be constrained to maintain numerical stability. It is also computationally demanding for a high dimensional surface. We therefore employed a multi-grid numerical scheme that introduces a hierarchical representation of the data in multiple scales and propagates the solutions from the coarse scale to the fine scale in order to achieve computational efficiency.

4. Experimental Results

We start with simple, but demonstrative synthetic images both in 2D and 3D for demonstrating the efficiency and the robustness of our algorithm. Following that the real patient data is used for further validation.

4.1. Synthetic data

We have comprared the accuracy of registration of our proposed scheme with the ICP scheme. The original 2D star shape (image size: 200 $\times$ 200 pixels) shwon in Figure 1(a) is first deformed (see Figure 1(e)) by adding Gaussian noise on the boundary. At the same time, the 33 noisy contour points are also generated by adding Gaussian noise (2%, 6% and 10% standard deviation of contour points) to the original points, respectively. The qualitative results of shape reconstruction and registration between deformed star shape and each noisy point set are shown in Figure 1(b)-(d) for ICP scheme and in Figure 1(f)-(h) for the proposed scheme. For the quantitative error analysis, we measure the mean Euclidean distance between the reconstructed surface and the given data points for varying degree of Gaussian noise. It is clear from Figure 2 that the proposed scheme outperforms the ICP.

Similarly, the comparative performance of the proposed scheme for a 3D synthetic image is shown in Figure 3, where the image size is 60 $\times$ 60 $\times$ 80 pixels. The original shape is generated in (a) and deformed shape is shown in (f). The 282 noisy contour points are generated by adding Gaussian noise (3%, 6%, 9% and 12% standard deviation of contour points) to the original points, respectively. The results using our algorithm are presented in Figure 3 (g)-(j)

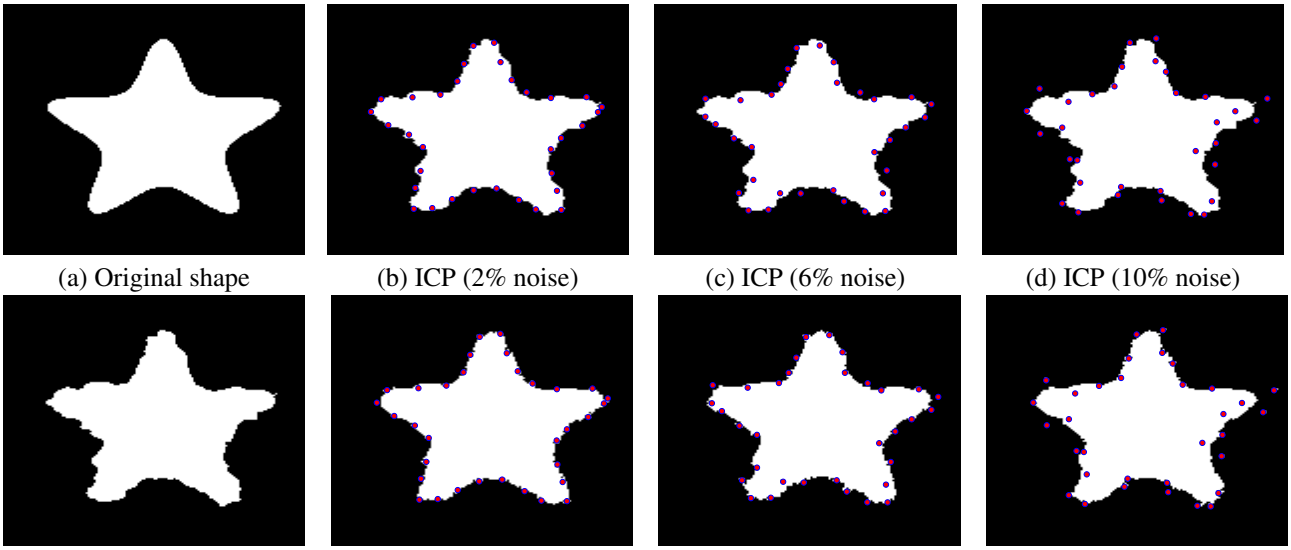

(a) Original shape (b) ICP (2% noise) (c) ICP (6% noise) (d) ICP (10% noise)

(e) Deformed shape (f) Our Method (2% noise) (g) Our Method (6% noise) (h) Our Method (10% noise)

Figure 1. The shape reconstruction results for a synthetic 2D star shape (a) Original shape, (b)-(d) ICP results using different Gaussian noise levels, (e) Deformed shape, and (f)-(h) Results of our proposed method using different Gaussian noise levels.

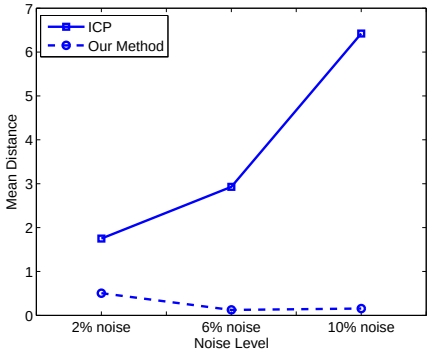

Figure 2. The Mean Distance between the reconstructed surface and the given data points for the 2D star shape exmaple.

and the results of ICP are presented in Figure 3 (b)-(e). The resulting shapes are deformed due to the point data fidelity term. The mean distances are measured for comparison of the accuracy. As shown in Figure 4, our algorithm achieved better result than the ICP scheme.

4.2. Patient data

Finally, a set of patient data is used for further validation. 3D pre-operative contrast-enhanced MR angiography (MRA) is performed to delineate the endocardial boundaries of the left atrium and pulmonary veins. The voxel size is $0.78125 \times 0.78125 \times 1.5$mm and 45 slices are used in our experiment. We obtained MRA and 250 EAM data points of the same patient. The EAM data consists of the carto points imported from the CARTO-XP, including the measuring points as well as ablation points.

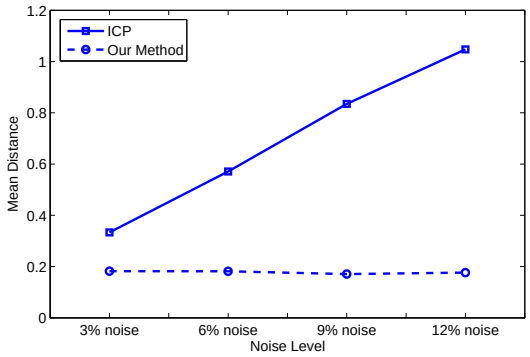

Figure 4. Mean Distance between the reconstructed surface and the given data points from a 3D jar exmaple.

After delineating and removing the unwanted regions, such as left ventricle (LV) and other small veins, we reconstruct the 3D model as shown in Figure 5 using ITK-SNAP

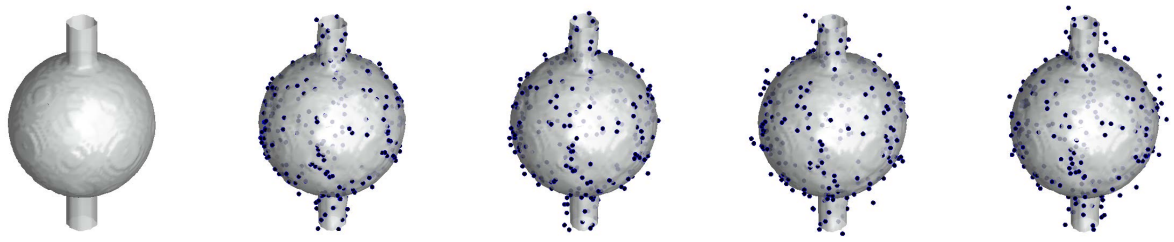

(a) Original shape (b) ICP (3% noise) (c) ICP (6% noise) (d) ICP (9% noise) (e) ICP (12% noise)

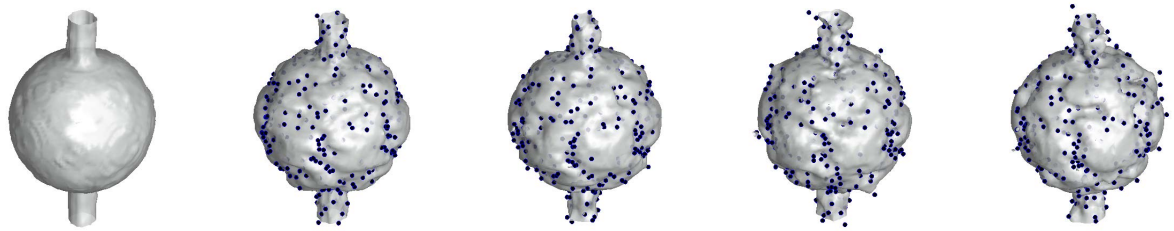

(f) Deformed shape (g) Ours (3% noise) (h) Ours (6% noise) (i) Ours (9% noise) (j) Ours (12% noise)

Figure 3. The shape reconstruction results for a synthetic 3D image, (a) Original shape, (b)-(e) ICP result using different Gaussian noise levels, (f) Deformed shape, and (g)-(j) Result of our method using different Gaussian noise levels.

[21] and Matlab software. Thereafter, two steps of registration process are applied for ICP method. First, we perform the landmark registration using three junctions between LA and pulmonary veins: LA-LIPV, LA-LSPV, and LA-RSPV. These points are used for initial pose of the subsequent registration. Secondly, the surface registration using ICP is performed to further refine the accuracy. The resulting image is shown in Figure 6(a).

To validate our algorithm, on the other hand, the optimal surface is reconstructed using 250 EAM data points by incorporating a heart shape prior from pre-operative MRA. By minimizing the given energy functional, the final surface is obtained in Figure 6(b). Blue points represent EAM data points and red points represent ablation points. Blurred points are located inside. The quantitative evaluations are obtained by using the 3D LA surface with points and the mean distances of the EAM and ablation points from the LA surface are measured in the Table 1. The table shows that our approach achieved better result than ICP method.

5. Conclusion and Future Work

In this paper, we presented a novel image integration technique for the use of catheter ablation. This novel method enabled reconstruction and registration simultaneously and achieved better performance than existing method in terms of accuracy. Clinically this has the potential to improve efficacy and safety of Atrial Fibrillation ablation by creating a more precise integration of EAM data and 3D imaging. However we have limitations in that larger studies using multiple data sets is essential to gauge its actual utility and only a single and static shape template is considered as a shape prior knowledge.

In the future work, we shall incorporate a more rich shape model using temporal shape template. For this, dynamic and spatio-temporal cardiac shape analysis is requried, which will make the current integration method more precise and meaningful.

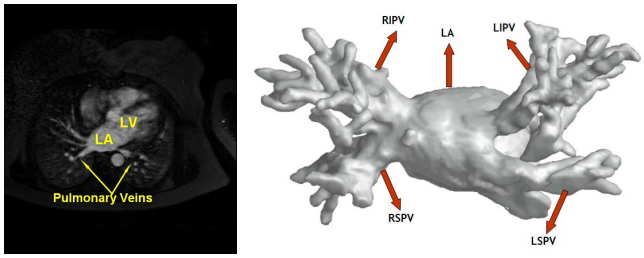

(a) MRA of LA (b) 3D Reconstruction

Figure 5. The 3D patient data.

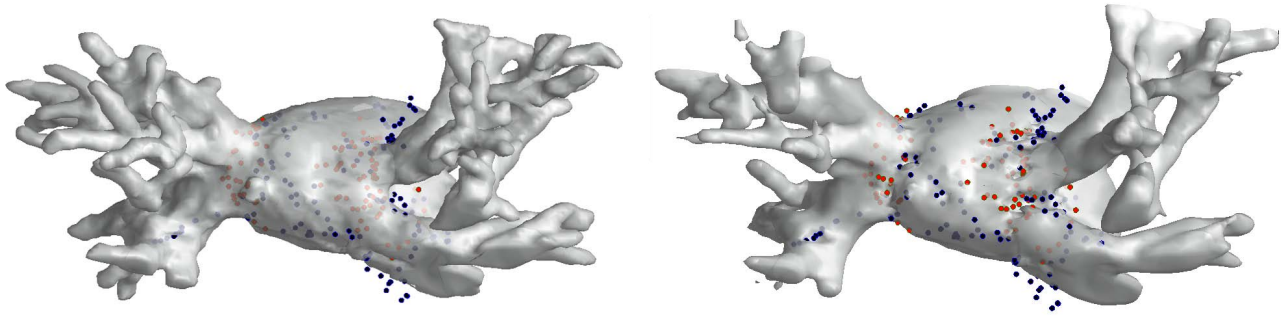

(a) ICP (b) Our method

Figure 6. The surface registration results for the patient data.

Table 1. Comparison of two methods

	ICP	Our Method
EAM point mean distance	4.5087mm	2.4113mm
Ablation point mean distance	3.2046mm	2.0921mm

References

[1] N. Amenta and M. Bern. Surface reconstruction by voronoi filtering. *Discrete and Computational Geometry*, 22(4):481–504, 1999.

[2] P. J. Besl and N. D. McKay. A method for registration of 3-d shapes. *IEEE Trans. Pattern Anal. Mach. Intell.*, 14(2):239–256, 1992.

[3] T. Chan and L. Vese. Active contours without edges. *IEEE Transactions on Image Processing*, 10(2):266–277, February 2001.

[4] D. Chetverikov, D. Svirko, D. Stepanov, and P. Krsek. The trimmed iterative closest point algorithm. *International Conference on Pattern Recognition*, 03:30545, 2002.

[5] A. Dervieux and F. Thomasset. A finite element method for the simulation of Rayleigh-Taylor instability. *Lecture Notes in Mathematics*, 771:145–159, 1979.

[6] A. Dervieux and F. Thomasset. Multifluid incompressible flows by a finite element method. In W. Reynolds and R. MacCormack, editors, *Seventh International Conference on Numerical Methods in Fluid Dynamics*, volume 141 of *Lecture Notes in Physics*, pages 158–163, June 1980.

[7] J. Dong, H. Calkins, S. B. Solomon, S. Lai, D. Dalal, A. Lardo, E. Brem, A. Preiss, R. D. Berger, H. Halperin, and T. Dickfeld. Integrated Electroanatomic Mapping With Three-Dimensional Computed Tomographic Images for Real-Time Guided Ablations. *Circulation*, 113(2):186–194, 2006.

[8] H. Edelsbrunner. Shape reconstruction with delaunay complex. In *LATIN '98: Proceedings of the Third Latin American Symposium on Theoretical Informatics*, pages 119–132, London, UK, 1998. Springer-Verlag.

[9] E. Heist, J. Chevalier, G. Holmvang, and et al. Factors affecting error in integration of electroanatomic mapping with ct and mr imaging during catheter ablation of atrial fibrillation. *Journal of Interventional Cardiac Electrophysiology*, 17(1):21–27, October 2006.

[10] H. Hoppe, T. DeRose, T. Duchamp, J. McDonald, and W. Stuetzle. Surface reconstruction from unorganized points. *Computer Graphics*, 26(2):71–78, 1992.

[11] Z. Malchano. Image guidance in cardiac electrophysiology. Master's thesis, Massachusette Institute of Technology, Boston, MA, June 2006.

[12] T. Masuda, K. Sakaue, and N. Yokoya. Registration and integration of multiple range images for 3-d model construction. In *Pattern Recognition, 1996., Proceedings of the 13th International Conference on*, pages 879–883, 1996.

[13] S. Osher and J. Sethian. Fronts propagating with curvature dependent speed: algorithms based on the Hamilton–Jacobi formulation. *J. of Comp. Physics*, 79:12–49, 1988.

[14] C. Pappone, S. Rosanio, G. Orte, and et al. Circumferential radiofrequency ablation of pulmonary vein ostia. *circulation*, 102:2619–2628, November 2000.

[15] K. Pulli. Multiview registration for large data sets. In *Inlt. Conf. on 3D Digital Imaging and Modeling*, pages 160–168, 1999.

[16] I. B. Ray and E. Heist. Treating atrial fibrillation. what is the consensus now? *Postgraduate medicine*, 118(4), October 2005.

[17] V. Reddy, Z. Malchano, G. Holmvang, and et al. Integration of cardiac magnetic resonance imaging with three-dimensional electroanatomic mapping to guide left ventricular catheter manipulation: feasibility in a porcine model of healed myocardial infarction. *J Am Coll Cardiol*, 44(11):2202–2213, 2004.

[18] D. Rogers. *An Introduction to NURBS: With Historic Perspective*. Morgan Kaufmann Publisher Inc., San Francisco, CA, 2001.

[19] S. Rusinkiewicz and M. Levoy. Efficient variants of the ICP algorithm. In *Proceedings of the Third Intl. Conf. on 3D Digital Imaging and Modeling*, pages 145–152, 2001.

[20] J. Sethian. *Level Set Methods and Fast Marching Methods: Evolving Interfaces in Computational Geometry*. Cambridge University Press, 1998.

[21] P. A. Yushkevich, J. Piven, H. Cody, S. Ho, J. C. Gee, and G. Gerig. User-guided level set segmentation of anatomical

structures with ITK-SNAP. *Insight Jounral*, 1, 2005. Special Issue on ISC/NA-MIC/MICCAI Workshop on Open-Source Software.

[22] H. Zhao, T. Chan, B. Merriman, and S. Osher. A variational level set approach to multiphase motion. *J. Comput. Phys.*, 127:179–195, 1996.

[23] H. Zhao, S. Osher, and R. Fedkiw. Fast surface reconstruction using the level set method. *1st IEEE Workshop on Variational and Level Set Methods, 8th ICCV, Vancouver*, pages 194–202, 2001.